THE AMERICAN SOCIETY OF MECHANICAL ENGINEERS
345 E. 47th St., New York, N.Y. 10017

97-GT-186

A COUPLED MODE ANALYSIS OF UNSTEADY MULTISTAGE FLOWS IN TURBOMACHINERY

Peter D. Silkowski* and Kenneth C. Hall†
Department of Mechanical Engineering and Materials Science
Duke University
Durham, North Carolina

ABSTRACT

A computational method is presented for predicting the unsteady aerodynamic response of a vibrating blade row which is part of a multistage turbomachine. Most current unsteady aerodynamic theories model a single blade row isolated in an infinitely long duct. This assumption neglects the potentially important influence of neighboring blade rows. The present 'coupled mode' analysis is an elegant and computationally efficient method for modelling neighboring blade row effects. Using this approach, the coupling between blade rows is modelled using a subset of the so-called spinning modes, i.e. pressure, vorticity, and entropy waves which propagate between the blade rows. The blade rows themselves are represented by reflection and transmission coefficients. These coefficients describe how spinning modes interact with, and are scattered by, a given blade row. The coefficients can be calculated using any standard isolated blade row model; here we use a linearized full potential flow model together with rapid distortion theory to account for incident vortical gusts. The isolated blade row reflection and transmission coefficients, inter-row coupling relationships, and appropriate boundary conditions are all assembled into a small sparse linear system of equations which describes the unsteady multistage flow. A number of numerical examples are presented to validate the method and to demonstrate the profound influence of neighboring blade rows on the aerodynamic damping of a cascade of vibrating airfoils.

1. INTRODUCTION

Unsteady fluid motion is essential to gas turbine engine operation. Only through unsteady flow processes can a machine do work on a fluid to increase its total enthalpy. This unsteadiness is provided in compressors and turbines by relative motion of adjacent stators and rotors. Unfortunately, this motion also produces undesirable aeroacoustic and aeroelastic phenomena, i.e. tonal noise and forced blade vibrations induced by rotor/stator interactions. Furthermore, the aeroelastic (flutter) stability of a rotor can be profoundly influenced by the presence of nearby stators and rotors. In this paper, we investigate the aeroelastic stability of a compressor rotor which is part of a larger multistage compressor.

Unsteady aerodynamic theories for use in turbomachinery aeroelastic prediction systems have progressed significantly over the past four decades. Several recent review articles chronicle the development of these theories (Verdon, 1987, Verdon, 1993; Whitehead, 1987; Marshall & Imregun, 1996). The available theories can be classified roughly into three groups: classical or linear methods, time-linearized theories, and nonlinear time-domain simulations.

In the classical approach, simplifying assumptions are made which reduce the equations governing the unsteady flow to linear constant coefficient equations for the unknown unsteady perturbation flow. For example, the airfoils of the cascade are usually replaced by flat plates which do not turn the mean flow. These simplified governing equations are then solved analytically or semi-analytically. This approach has been applied to incompressible flows (Whitehead, 1960), subsonic flows (Whitehead, 1970; Smith,1972), and supersonic flows (Verdon & McCune, 1975; Nagashima & Whitehead, 1977; Adamczyk & Goldstein, 1978).

Using the time-linearized approach, the governing equations are linearized about a nonlinear steady operating condition. The unsteady small-disturbance quantities are assumed to be harmonic in time, i.e. unsteady quantities are proportional to $\exp(j\omega t)$, so that the time derivative $\partial/\partial t$ is replaced by $j\omega$. The resulting linear variable coefficient equations are then discretized on a computational grid using conventional finite element or finite volume techniques and solved numerically. The time-linearized approach is computationally efficient, and has been applied to a range of flow models including the two-dimensional potential equa-

*Currently employed by Pratt & Whitney Aircraft, East Hartford, CT 06108.
†Member ASME.

Presented at the International Gas Turbine & Aeroengine Congress & Exhibition
Orlando, Florida — June 2–June 5, 1997
This paper has been accepted for publication in the Transactions of the ASME
Discussion of it will be accepted at ASME Headquarters until September 30, 1997

tions (Verdon & Caspar, 1982; Whitehead, 1990; Hall, 1993), the two-dimensional Euler equations (Hall & Crawley, 1989; Hall & Clark, 1993; Holmes & Chuang, 1993), the three-dimensional Euler equations (Hall & Lorence, 1993), and the two-dimensional Navier-Stokes equations (Clark & Hall, 1995).

Finally, investigators have developed nonlinear time-domain simulations of unsteady flows in cascades. Using this approach, no simplifying assumptions are made regarding the size of the unsteady disturbance. Instead, the governing fluid dynamic equations, which are nonlinear, are simply marched in time to simulate the unsteady flow. The approach has been applied to the two-dimensional Euler equations (Huff *et al.*, 1991; Giles, 1988a; Giles, 1988b; He, 1990) and the three-dimensional Euler equations (Gerolymos, 1993). This approach has the advantage that it is reasonably straightforward to implement, and can model nonlinearities. However, computational times are usually quite large, on the order of two orders of magnitude larger than the time-linearized approach.

Unfortunately, despite many years of development, the accurate and reliable prediction of unsteady aerodynamic forces acting on turbomachinery blades remains elusive. The correlation of theory with experiment is often less than satisfactory (Bölcs & Fransson, 1986), especially when viewed next to the great success investigators have had in predicting steady flows.

We believe there are two main reasons why current theories show poor correlation with experiment, both of which are related to the special physics of unsteady flows. First, most unsteady flow analyses are two-dimensional, or at best quasi-three-dimensional. The unsteady flow is calculated on a two-dimensional axisymmetric streamsheet whose radial thickness varies as a function of axial location. Steady flows are routinely calculated quite accurately using this sort of analysis. However, the unsteady flow equations admit acoustic wave solutions making the problem inherently three-dimensional since acoustic waves will travel in all directions. Quoting Holmes and Chuang (1993), "There is absolutely no reason to believe that unsteady disturbances will obligingly confine themselves to the [quasi-three-dimensional] mean flow streamsheets! Cases in which [two-dimensional] or [quasi-three-dimensional] unsteady flow codes give accurate results will be relatively rare." Recent work by Hall & Lorence (1993) tends to confirm this hypothesis.

The second main reason for these discrepancies is that nearly all of the current unsteady aerodynamic theories model a single blade row in an infinitely long duct, ignoring potentially important multistage effects. However, unsteady flows are made up of acoustic, vortical, and entropic waves. These waves provide a mechanism for the rotors and stators of multistage machines to communicate with one another. For example, consider the case of a row of vibrating rotor blades (see Fig. 1). The blades will respond aerodynamically, producing acoustic, vortical, and entropic waves which propagate away from the rotor. Some of these waves will then impinge on the neighboring stators. The stators will in turn respond aerodynamically, again producing waves, some of which will impinge upon the original rotor, and so on. In other words, wave behavior makes unsteady flows fundamentally three-dimensional and multistage.

Recently, a number of investigators have studied unsteady multistage flows. The most common approach is to perform a direct

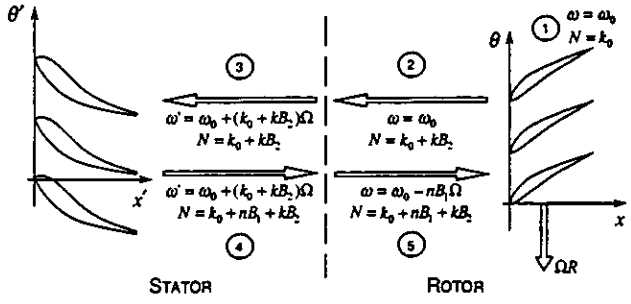

Figure 1: Kinematics of mode scattering and frequency shifting.

simulation. For example, Giles (1988a, 1988b) has time-marched the Euler equations to compute wake/rotor and rotor/stator interactions. For the latter, two computational grids are generated, one for the rotor and one for the stator, with a common interface. The Euler equations are then time marched. At each time step, information at the rotor/stator interface is exchanged, and the position of the rotor is updated. Rai (1989a, 1989b) used a similar technique to study viscous rotor/stator interaction in turbines. One problem with this approach is that many passages of the rotor and stator must be used if the blade counts in the two blade rows are not equal, making the method prohibitively expensive. Rai (1989a, 1989b) simply altered the geometry of one of the blade rows to force the blade counts to be equal, an approach of questionable validity, especially for unsteady flows where the blade counts have a strong influence on the possible tones or frequencies present in the solution. Giles (1988a, 1988b), on the other hand, used an elegant 'time-inclining' technique whereby a space-time transformation is made on the governing flow equations which allows the ratio of blades to be altered, for example from 11:9 to 1:1. Unfortunately, the method has not yet been extended to flows in multiple stages.

A few researchers have modelled multistage flows using frequency domain techniques. Kaji & Okazaki (1970) studied rotor/stator interactions using an acceleration potential technique. They distributed pressure doublets on flat-plate rotor and stator blades. The strengths of the doublets were found by satisfying the no-through-flow condition on the airfoils. However, Kaji & Okazaki assumed the doublet strengths were harmonic in time with a single interblade phase angle in each blade row. In other words, the two blade rows were coupled by a single family of spinning modes, i.e. acoustic and vortical waves with a single temporal frequency and circumferential wavenumber. Hanson (1992) later applied a similar technique to acoustic problems, using vortex singularities with multiple spinning modes.

Hanson (1993), using an alternative approach suggested by Hall in a 1988 unpublished report, characterized the rotor and stator by reflection and transmission coefficients which describe the response of an isolated blade row to incident vortical or acoustic waves (spinning modes). Hanson used Smith's (1972) method to compute these coefficients. A small set of linear equations can then be assembled which describes how the two blade rows behave when put together into a single stage. Hanson used this method to study the influence of 'mode trapping' on the aeroacoustic behavior of a single stage. Buffum (1993) later used a similar technique to investigate the aeroelastic stability of a one and one-half stage compressor. How-

ever, Buffum retained only cut-on (superresonant) acoustic modes, and used only a single spinning mode in his model. Concurrently to Hanson's (1993) work, Hall & Silkowski (1995) also developed a coupled mode approach to analyze unsteady flows associated with flutter and forced response of multistage machines composed of flat-plate airfoils, and analyzed machines with as many as three and one-half stages.

In this paper, the coupled mode analysis is extended and applied to the problem of computing the aerodynamic damping of a compressor rotor which is part of a multistage compressor composed of realistic airfoils. That is to say, the blades have camber and thickness, and the blade rows do significant turning of the flow. We show that the aerodynamic damping of a blade row which is part of a multistage machine will, in general, be significantly different than that predicted using an isolated blade row model.

The coupled mode analysis has a number of features that make it desirable for use in aeroelastic and aeroacoustic design/analysis systems. For example, the method is computationally very efficient, especially when compared to conventional time-marching simulations. Furthermore, once a single nominal multistage flow has been computed, certain design parametric studies can be performed with virtually no additional computational expense.

2. THEORY

The coupled mode analysis is divided into two parts. First, there is a framework for describing how blade rows interact with one another via so-called spinning modes. In Section 2.1, we describe this framework. Second, a linear or time-linearized unsteady aerodynamic analysis is required to determine reflection and transmission coefficients which characterize the behavior of the individual blade rows. In Section 2.2, we describe the time-linearized theory used in the present investigation, a linearized full potential flow solver along with rapid distortion theory to describe the motion of vorticity through the blade row.

2.1. Coupled Mode Analysis

2.1.1. Kinematics of Mode Scattering and Frequency Shifting. In the present work, we assume that the flow through a multistage compressor or turbine is inviscid, non-heat conducting, and two-dimensional. Therefore, the flow is governed by the nonlinear two-dimensional Euler equations. The state of the flow is completely described by the vector of primitive flow variables $\hat{\mathbf{U}}$ given by

$$\hat{\mathbf{U}}(x,y,t) = \begin{Bmatrix} \hat{\rho}(x,y,t) \\ \hat{U}(x,y,t) \\ \hat{V}(x,y,t) \\ \hat{P}(x,y,t) \end{Bmatrix} \tag{1}$$

where $\hat{\rho}$, $\hat{U}$, $\hat{V}$, and $\hat{P}$ are the density, axial velocity, circumferential velocity, and pressure, respectively, x and y are the axial and circumferential coordinates, and t is time. The angular distance θ is just equal to y/R where R is the radius of the annulus.

Consider the single stage shown in Fig. 1 for the case where the airfoils of the rotor vibrate periodically with small amplitude and frequency ω_0. The resulting unsteadiness in the flow is assumed to be small compared to the mean flow. Thus, the flow may be split into a nonlinear mean or steady part plus an unsteady small-perturbation part, i.e.

$$\hat{\mathbf{U}}(x,y,t) = \mathbf{U}(x,y) + \mathbf{u}(x,y,t) \tag{2}$$

The unsteady flow $\mathbf{u}(x,y,t)$ is described by the linearized Euler equations (Hall & Crawley, 1989) – linear variable coefficient equations whose coefficients depend on the mean flow (see Section 2.2). Thus, unsteady solutions may be superposed. It will be useful to use this property to decompose the motion of the rotor into a sum of traveling waves, analyze each traveling wave mode separately, then superpose the resulting solutions. Hence, without loss in generality, we assume that the blades of the rotor vibrate in plunge with frequency ω_0 in a traveling wave with $N = k_0$ nodal diameters. Thus, the plunging velocity of the mth blade is given by

$$\dot{h}(m,t) = \dot{h}_0 \exp[j(\omega_0 t + m\sigma_0)] \tag{3}$$

where

$$\sigma_0 = \frac{2\pi k_0}{B_2} \tag{4}$$

is the interblade phase angle of the motion, $\dot{h}_0$ is the amplitude of the plunging velocity of the reference airfoil, and B_2 is the number of blades in the rotor (blade row number 2).

This traveling wave motion of the blades will give rise to unsteady fluid motion with frequency ω_0, and that also satisfies the complex periodicity condition

$$\mathbf{u}(x, y+G_2, t) = \mathbf{u}(x,y,t)\exp(j\sigma_0) \tag{5}$$

where G_2 is the circumferential spacing between blades on the rotor. Upstream and downstream of the rotor, Eq. (5) can be satisfied with solutions of the form

$$\mathbf{u}(x,\theta,t) = \sum_{k=-\infty}^{\infty} \overline{\mathbf{u}}_k(x)\exp\{j[(k_0 + kB_2)\theta + \omega_0 t]\} \tag{6}$$

where k is a mode order index which can take on all integer values, and $\overline{\mathbf{u}}_k(x)$ is a vector function to be determined.

In the inter-row regions, the mean (time-averaged) flow is uniform, or very nearly so. Thus, the linearized Euler equations reduce to constant coefficient equations. Substituting Eq. (6) into the (constant coefficient) linearized Euler equations, one finds that $\overline{\mathbf{u}}_k(x)$ has exponential behavior, so that

$$\mathbf{u}(x,\theta,t) = \sum_{k=-\infty}^{\infty}\sum_{i=1}^{4} v_{i,k}\mathbf{q}_{i,k}\exp\{j[\alpha_{i,k}x + (k_0 + kB_2)\theta + \omega_0 t]\} \tag{7}$$

In words, the kth spinning mode has N nodal diameters, where $N = k_0 + kB_2$. The spinning mode is composed of four waves with wavenumbers $\alpha_{i,k}$ and eigenvectors $\mathbf{q}_{i,k}$ (Hall & Crawley, 1989). The constant $v_{i,k}$ describes how much of each eigenvector is present in the solution. The four waves correspond to an upstream moving pressure wave, a downstream moving pressure wave, a vorticity wave, and an entropy wave, with wavenumbers given by

$$\alpha_1 = \frac{U(\omega + \beta V) + C\sqrt{(\omega+\beta V)^2 - (C^2 - U^2)\beta^2}}{C^2 - U^2} \tag{8}$$

$$\alpha_2 = \frac{U(\omega+\beta V) - C\sqrt{(\omega+\beta V)^2 - (C^2-U^2)\beta^2}}{C^2-U^2} \quad (9)$$

$$\alpha_3 = -\frac{\beta V+\omega}{U} \quad (10)$$

$$\alpha_4 = -\frac{\beta V+\omega}{U} \quad (11)$$

where U and V are the mean flow axial and circumferential velocities, C is the mean speed of sound, and β_k is the circumferential wavenumber equal to σ_k/G_2 with $\sigma_k = \sigma_0 + 2\pi k$. (In Eqs. (8)–(11), the subscript k has been omitted for clarity.) Note that $\alpha_{3,k}$ and $\alpha_{4,k}$ are always real. However, $\alpha_{1,k}$ and $\alpha_{2,k}$ may be real or complex. When the wavenumbers are real, the waves are said to be 'superresonant' or 'cut-on' and the waves propagate without attenuation; when the wavenumbers are complex, the waves are 'subresonant' or 'cut-off' and the waves are attenuated as they propagate. The boundary between these two conditions is known as acoustic resonance.

Note that an initial disturbance with k_0 nodal diameters will in general produce a response composed of outgoing waves with an infinite number of nodal diameters, $N = k_0 + kB_2$. This phenomenon is referred to as scattering. Each of these spinning modes, identified by the index k, have the same temporal frequency ω_0 when viewed in the rotor frame of reference. Such a group of spinning modes for a particular blade row will be referred to as a scatter group.

The individual waves (pressure, vorticity, and entropy) of the spinning modes that were created by the rotor vibration will propagate upstream or downstream through the duct, depending on the wavenumber. Some of the upstream traveling pressure waves will impinge on the upstream stator. When viewed in the stator frame of reference, however, the frequency will be shifted. To show this, the coordinates (x,θ) fixed to the moving rotor can be related to the coordinates (x',θ') attached to the stator (see Fig. 1) by the transformation

$$x = x' - \Delta x \quad (12)$$

$$\theta = \theta' - \Delta\theta + \Omega t \quad (13)$$

where Δx is the axial distance between the stator and the rotor, $\Delta\theta$ is an angular location defining the relative clocking of the rotor and stator at time $t = 0$, and Ω is the rotation rate of the rotor. Substitution of Eqs. (12) and (13) into Eq. (7) gives

$$\mathbf{u}(x',\theta',t) = \sum_{k=-\infty}^{\infty}\sum_{i=1}^{4} v_{i,k}\mathbf{q}_{i,k}\exp\{\jmath[\alpha_{i,k}x' + (k_0+kB_2)\theta' + \omega_k' t]\} \times \exp\{\jmath[-\alpha_{i,k}\Delta x - (k_0+kB_2)\Delta\theta]\} \quad (14)$$

where $\omega_k' = \omega_0 + (k_0 + kB_2)\Omega$. Note that each of the members of the scatter group experiences a different 'Doppler' frequency shift when viewed in the stator frame of reference, with the frequency dependent on the index k associated with the scattering in the rotor frame.

The upstream traveling waves of this scatter group will impinge on the stator, which in turn will give rise to an unsteady aerodynamic response. Following the same logic outlined for the rotor, the kth spinning mode will produce scattered reflected and transmitted waves with nodal diameters $N = k_0 + nB_1 + kB_2$, where B_1 is the number of stator blades and n takes on all integer values. In the stator frame of reference, these new waves will have frequencies given by

$$\omega_k' = \omega_0 + (k_0 + kB_2)\Omega \quad (15)$$

The reflected waves will impinge on the rotor. When viewed in the rotor frame of reference, however, the frequencies of the waves will again be shifted, so that

$$\omega_n = \omega_0 - nB_1\Omega \quad (16)$$

The waves impinging on the rotor will again produce reflected and transmitted waves, but no new nodal diameters will be produced. Thus, the response of the system to an initial disturbance with nodal diameters $N = k_0$ and frequency ω_0 will contain waves with nodal diameters $N = k_0 + nB_1 + kB_2$ and frequencies given by Eqs. (15) and (16). Note that the frequencies in the stator frame of reference depend on the index k associated with scattering of waves by the rotor, and the frequencies in the rotor frame of reference depend on the index n associated with scattering of waves by the stator.

Finally, for the cases considered in this paper, the mean background flow is subsonic, inviscid, irrotational, and homentropic. Furthermore, the original source of excitation is blade vibration. Under these circumstances, only acoustic and vortical disturbances will be generated, that is, the unsteady flow will also be homentropic. Therefore, for simplicity in the following, entropy waves are omitted. However, for nonhomentropic flows, entropy waves can be included in a straightforward extension of the method described below.

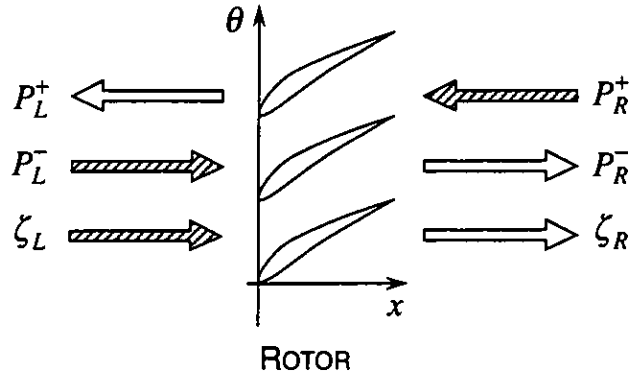

Figure 2: Incident pressure and vorticity waves (shaded) produce reflected and transmitted pressure and vorticity waves (unshaded).

2.1.2. Global System Description. Having outlined the kinematics of mode scattering and frequency shifting in a multistage machine, we next consider in detail the interaction of spinning modes with individual blade rows. The fluid/blade row interaction can be described in terms of incident and outgoing waves (see Fig. 2). We know from the above discussion that incident acoustic and vortical waves (P_R^+, P_L^-, and ζ_L) from a single spinning mode

will generate outgoing acoustic and vortical waves (P_R^-, P_L^+, and ζ_R) with all nodal diameters of the scatter group. Here, P^+, P^-, and ζ are the complex magnitudes of acoustic and vortical waves, replacing the less descriptive v_i notation of Eqs. (7) and (14). The 'L' and 'R' notation signify left (upstream) and right (downstream) sides of the blade row. The '+' and '−' notation signify upstream and downstream traveling waves. Conversely, outgoing waves for a particular nodal diameter are generated by incident waves from every member of the scatter group. Hence, for a rotor, for a specific (n, k) spinning mode,

$$\begin{Bmatrix} P_L^+ \\ P_R^- \\ \zeta_R \end{Bmatrix}_{nk} = \sum_{j=-\infty}^{\infty} \begin{bmatrix} w_{11} & w_{12} & w_{13} \\ w_{21} & w_{22} & w_{23} \\ w_{31} & w_{32} & w_{33} \end{bmatrix}_{nknj} \begin{Bmatrix} P_R^+ \\ P_L^- \\ \zeta_L \end{Bmatrix}_{nj} + \begin{Bmatrix} b_1 \\ b_2 \\ b_3 \end{Bmatrix}_{nk} \tag{17}$$

where the matrix $\mathbf{w}_{nknj}$ is a matrix of reflection and transmission coefficients describing how incident (n, j) waves scatter into (n, k) waves. The vector $\mathbf{b}_{nk}$ is an an inhomogeneous term arising from the imposition of an external disturbance. For example, $\mathbf{b}_{nk}$ might describe the (n, k) waves generated by a prescribed traveling wave blade motion with frequency ω_0 and k_0 nodal diameters. The reflection/transmission matrix $\mathbf{w}_{nknj}$ and the inhomogeneous vector $\mathbf{b}_{nk}$ are obtained using classical or time-linearized unsteady aerodynamic theories (see Section 2.2).

It will be convenient to rearrange Eq. (17) in terms of fluid waves on the left (upstream) side and right (downstream) side of the blade row instead of incident and outgoing waves. Rearranging Eq. (17) gives

$$\sum_{j=-\infty}^{\infty} \left[\mathbf{A}^i_{nknj} \mathbf{v}^i_{L,nj} + \mathbf{B}^i_{nknj} \mathbf{v}^i_{R,nj} \right] = \mathbf{b}^i_{nk} \tag{18}$$

where i is the blade row number,

$$\mathbf{v}^i_{L,nj} = \begin{Bmatrix} P_L^+ \\ P_L^- \\ \zeta_L \end{Bmatrix}_{nj}, \quad \mathbf{v}^i_{R,nj} = \begin{Bmatrix} P_R^+ \\ P_R^- \\ \zeta_R \end{Bmatrix}_{nj} \tag{19}$$

and

$$\mathbf{A}^i_{nknj} = \begin{bmatrix} \delta_{jk} & -w_{12} & -w_{13} \\ 0 & -w_{22} & -w_{23} \\ 0 & -w_{32} & -w_{33} \end{bmatrix}_{nknj} \tag{20}$$

$$\mathbf{B}^i_{nknj} = \begin{bmatrix} -w_{11} & 0 & 0 \\ -w_{21} & \delta_{jk} & 0 \\ -w_{31} & 0 & \delta_{jk} \end{bmatrix}_{nknj} \tag{21}$$

where δ_{jk} is the Kronecker delta function. A similar set of equations can be developed for the stator.

Next, a set of equations is required to model the coupling provided by the spinning modes in the inter-row region. For the stator/rotor example shown in Fig. 1, a wave leaving the rotor is equivalent to a wave entering the stator. Said another way, the $\mathbf{v}_R$ quantities of the stator must be related to the $\mathbf{v}_L$ quantities of the rotor. Therefore,

$$\mathbf{E}_{nk} \mathbf{v}^1_{R,nk} + \mathbf{v}^2_{L,nk} = 0 \tag{22}$$

with

$$\mathbf{E}_{nk} = \begin{bmatrix} -e^{j\alpha_{1,nk}\Delta x} & 0 & 0 \\ 0 & -e^{j\alpha_{2,nk}\Delta x} & 0 \\ 0 & 0 & -e^{j\alpha_{3,nk}\Delta x} \end{bmatrix} \tag{23}$$

where for simplicity the clocking index $\Delta\theta$ is taken to be zero. Note that Eqs. (22) and (23) are based on the assumption that the time-averaged mean flow is uniform at some axial location between the blade rows, a condition which may be only approximately satisfied for very closely spaced blade rows.

Finally, one must specify any acoustic or vortical waves which originate upstream or downstream of the multistage machine. For the two blade row problem,

$$\mathbf{C} \mathbf{v}^1_{L,nk} + \mathbf{D} \mathbf{v}^2_{R,nk} = \mathbf{d}_{nk} \tag{24}$$

where

$$\mathbf{C} = \begin{bmatrix} 0 & 0 & 0 \\ 0 & 1 & 0 \\ 0 & 0 & 1 \end{bmatrix}, \quad \mathbf{D} = \begin{bmatrix} 1 & 0 & 0 \\ 0 & 0 & 0 \\ 0 & 0 & 0 \end{bmatrix} \tag{25}$$

and $\mathbf{d}_{nk}$ is a vector containing the complex magnitudes of the incoming pressure and vorticity disturbances. For the flutter problem, $\mathbf{d}_{nk}$ is set to zero.

Equations (18), (22), and (24) can be assembled into a small sparse matrix equation of the form given by Eq. (26) (see page following). Shown is the form of the matrix equation when the modes (n,k) = (0,0), (0,1), (1,0), and (1,1) are used for a single stage. Note that the system of equations is truncated. In principle, an infinite set of spinning modes must be included in the model to obtain the exact solution. In practice, however, only a few of the many possible modes are needed to obtain solutions with engineering accuracy. Also note the nonzero off-diagonal superblocks in Eq. (26). These are a result of mode scattering.

Although presented for a single stage, the above analysis easily generalizes to multiple stages. Consider a multistage machine with M blade rows. The number of blades in each blade row is B_1, B_2, B_3, ..., B_M, with rotors having even indices. If the original disturbance has n_0 nodal diameters and frequency ω_0 in the rotating frame of reference, then the resulting unsteady flow will contain spinning modes with N nodal diameters where

$$N = n_0 + \sum_{i=1}^{M} n_i B_i \tag{27}$$

with each n_i taking on all integer values. The corresponding frequencies of the spinning modes in the stationary frame are

$$\omega_{n2,n4,n6,\ldots} = \omega_0 + \Omega \left(n_0 + \sum_{i \text{ even}} n_i B_i \right) \tag{28}$$

Similarly, in the rotating frame, the frequencies of the spinning modes are given by

$$\omega_{n1,n3,n5,\ldots} = \omega_0 - \Omega \sum_{i \text{ odd}} n_i B_i \tag{29}$$

$$
\left[\begin{array}{cccc|c}
\mathbf{A}^1_{0000}\,\mathbf{B}^1_{0000} & & \mathbf{A}^1_{0010}\,\mathbf{B}^1_{0010} & & \\
\mathbf{E}_{00}\quad \mathbf{I} & & & & \\
\mathbf{A}^2_{0000}\,\mathbf{B}^2_{0000} & \mathbf{A}^2_{0001}\,\mathbf{B}^2_{0001} & & & \\
\mathbf{C}\qquad\quad \mathbf{D} & & & & \\
\hline
 & \mathbf{A}^1_{0101}\,\mathbf{B}^1_{0101} & & \mathbf{A}^1_{0111}\,\mathbf{B}^1_{0111} & \\
 & \mathbf{E}_{01}\quad \mathbf{I} & & & \\
\mathbf{A}^2_{0100}\,\mathbf{B}^2_{0100} & \mathbf{A}^2_{0101}\,\mathbf{B}^2_{0101} & & & \\
 & \mathbf{C}\qquad\quad \mathbf{D} & & & \\
\hline
\mathbf{A}^1_{1000}\,\mathbf{B}^1_{1000} & & \mathbf{A}^1_{1010}\,\mathbf{B}^1_{1010} & & \\
 & & \mathbf{E}_{10}\quad \mathbf{I} & & \\
 & & \mathbf{A}^2_{1010}\,\mathbf{B}^2_{1010} & \mathbf{A}^2_{1011}\,\mathbf{B}^2_{1011} & \\
 & & \mathbf{C}\qquad\quad \mathbf{D} & & \\
\hline
 & \mathbf{A}^1_{1101}\,\mathbf{B}^1_{1101} & & \mathbf{A}^1_{1111}\,\mathbf{B}^1_{1111} & \\
 & & & \mathbf{E}_{11}\quad \mathbf{I} & \\
 & & \mathbf{A}^2_{1110}\,\mathbf{B}^2_{1110} & \mathbf{A}^2_{1111}\,\mathbf{B}^2_{1111} & \\
 & & & \mathbf{C}\qquad\quad \mathbf{D} &
\end{array}\right]
\left[\begin{array}{c}
\mathbf{v}^1_{L,00} \\ \mathbf{v}^1_{R,00} \\ \mathbf{v}^2_{L,00} \\ \mathbf{v}^2_{R,00} \\ \hline
\mathbf{v}^1_{L,01} \\ \mathbf{v}^1_{R,01} \\ \mathbf{v}^2_{L,01} \\ \mathbf{v}^2_{R,01} \\ \hline
\mathbf{v}^1_{L,10} \\ \mathbf{v}^1_{R,10} \\ \mathbf{v}^2_{L,10} \\ \mathbf{v}^2_{R,10} \\ \hline
\mathbf{v}^1_{L,11} \\ \mathbf{v}^1_{R,11} \\ \mathbf{v}^2_{L,11} \\ \mathbf{v}^2_{R,11}
\end{array}\right]
=
\left[\begin{array}{c}
\mathbf{b}^1_{00} \\ \mathbf{0} \\ \mathbf{b}^2_{00} \\ \mathbf{d}_{00} \\ \hline
\mathbf{b}^1_{01} \\ \mathbf{0} \\ \mathbf{b}^2_{01} \\ \mathbf{d}_{01} \\ \hline
\mathbf{b}^1_{10} \\ \mathbf{0} \\ \mathbf{b}^2_{10} \\ \mathbf{d}_{10} \\ \hline
\mathbf{b}^1_{11} \\ \mathbf{0} \\ \mathbf{b}^2_{11} \\ \mathbf{d}_{11}
\end{array}\right]
\tag{26}
$$

2.2. Unsteady Aerodynamic Blade Row Model

The coupled mode analysis outlined above provides a flexible framework for solving unsteady flow problems in multistage compressors and turbines. In this section, the unsteady aerodynamic theory used to compute the unsteady flow in individual blade rows is summarized.

2.2.1. Rapid Distortion Theory. To begin, we assume that the flow is two-dimensional, inviscid, and homentropic, with constant total pressure P_T and total density ρ_T. Thus, the pressure $\hat{p}$ and density $\hat{\rho}$ are related through the condition

$$\frac{\hat{p}}{P_T} = \left(\frac{\hat{\rho}}{\rho_T}\right)^{\gamma} \tag{30}$$

where γ is the ratio of specific heats.

The unsteady flow is, in general, rotational. For convenience, we split the flow into a sum of irrotational (potential) and rotational (vortical) parts, so that

$$\mathbf{V}(x,y,t) = \nabla\hat{\Phi}(x,y,t) + \hat{\mathbf{V}}^R(x,y,t) \tag{31}$$

where $\hat{\Phi}(x,y,t)$ is a scalar velocity potential, and all the vorticity in the flow is contained in the rotational velocity $\hat{\mathbf{V}}^R(x,y,t)$. Furthermore, the unsteadiness in the flow is assumed to be small compared to the mean flow. Thus, we further split the flow into a mean or steady part, plus an unsteady small-disturbance part which is harmonic in time. It is assumed that the mean background flow is irrotational, but the unsteady flow may be rotational. Hence, the potential $\nabla\hat{\Phi}(x,y,t)$ and the rotational velocity $\hat{\mathbf{V}}^R(x,y,t)$ may be expressed as

$$\hat{\Phi}(x,y,t) = \Phi(x,y) + \phi(x,y)e^{j\omega t} \tag{32}$$

$$\hat{\mathbf{V}}^R(x,y,t) = \mathbf{v}^R(x,y)e^{j\omega t} \tag{33}$$

where $\Phi(x,y)$ is the mean flow potential, and $\phi(x,y)$, and $\mathbf{v}^R(x,y)$ are the complex amplitudes of the small disturbance potential and rotational velocities, respectively.

Integrating the conservation of momentum equation, one finds that the steady pressure is given by the steady Bernoulli equation

$$P = P_T\left[1 - \frac{\gamma-1}{2C_T^2}(\nabla\Phi)^2\right]^{\frac{\gamma}{\gamma-1}} \tag{34}$$

where $C_T^2 = \gamma P_T/\rho_T$. In general, the unsteady pressure is a function of both the perturbation potential ϕ and perturbation rotational velocity $\mathbf{v}^R$. Note, however, that the splitting given by Eqs. (31)–(33) is not unique. It is useful to constrain this splitting so that the perturbation pressure p is independent of the rotational velocity. In this case, integrating the unsteady momentum equation, one finds that the perturbation pressure is given by the linearized unsteady Bernoulli equation

$$p = -\overline{\rho}\frac{D\phi}{Dt} = -\overline{\rho}\left(\frac{\partial\phi}{\partial t} + \nabla\Phi\cdot\nabla\phi\right) \tag{35}$$

Next, Eqs. (30)–(35) are substituted into the continuity equation. Collecting terms of zeroth order and first order in the perturbation flow quantities, one obtains – after some considerable manipulation – the mean flow and linearized unsteady flow equations. The steady flow is governed by the nonlinear full potential equation, given by

$$\nabla^2\Phi = \frac{1}{C^2}\left[\frac{1}{2}\nabla\Phi\cdot\nabla(\nabla\Phi)^2\right] \tag{36}$$

where C is the steady flow speed of sound given by

$$C^2 = C_T^2\left[1 - \frac{\gamma-1}{2C_T^2}(\nabla\Phi)^2\right] \tag{37}$$

Note that the full potential equation is nonlinear in the unknown potential Φ.

Similarly, the time-linearized equations describing the unsteady flow – the linearized Euler equations for homentropic flow – are

$$\frac{D\mathbf{v}^R}{Dt} + \left(\mathbf{v}^R\cdot\nabla\right)\nabla\Phi = 0 \tag{38}$$

$$\frac{D}{Dt}\left(\frac{1}{C^2}\frac{D\phi}{Dt}\right) - \frac{1}{\bar{\rho}}\nabla\cdot(\bar{\rho}\nabla\phi) = \frac{1}{\bar{\rho}}\nabla\cdot\left(\bar{\rho}\mathbf{v}^R\right) \qquad (39)$$

Equation (38) describes the convection and distortion of the rotational velocity $\mathbf{v}^R$. Equation (39) is the usual linearized potential equation, but with a source term on the right-hand side to account for the fact that the rotational velocity $\mathbf{v}^R$ does not necessarily satisfy mass continuity. Note that Eqs. (38) and (39) are sequentially coupled, that is, one can first solve Eq. (38) for $\mathbf{v}^R$, then solve Eq. (39) for ϕ.

Goldstein (1978) showed that, remarkably, the rotational velocity may be expressed analytically in terms of the steady flow stream function Ψ and Lighthill's (1956) drift function Δ. The drift function Δ is essentially the time required for a fluid particle to convect from a reference point on a streamline to another point on the same streamline. Following Goldstein (1978) and Atassi & Grzedzinski (1989),

$$\mathbf{v}^R = [c_1(\Psi)\nabla\Delta + c_2(\Psi)\nabla\Psi]\exp[j(K_1\Delta + K_2\Psi)] \qquad (40)$$

where K_1 and K_2 are essentially wavenumbers, and are related algebraically to the axial and circumferential wavenumbers α and β. The functions c_1 and c_2 determine the amplitude of vorticity coming into the cascade. Goldstein's (1978) original formulation is singular for airfoils with stagnation points. Atassi & Grzedzinski (1989) later removed this singularity by a judicious choice of $c_1(\Psi)$ and $c_2(\Psi)$. Hall & Verdon (1991) and Lorence & Hall (1996) later used this modified formulation to compute unsteady flows in cascades.

2.2.2. Numerical Solution of the Steady Flow Field. The steady flow potential equation, Eq. (36), is solved numerically using a nonlinear variational finite element solver developed by Hall (1993). The computational grid used in this study is an H-grid composed of quadrilateral cells. Four-node isoparametric finite elements are used to discretize Bateman's (1930) variational principle for compressible flow. The resulting discretized equations take the form

$$\mathbf{N}(\Phi, \mathbf{X}) = 0 \qquad (41)$$

where $\mathbf{N}$ is a vector of nonlinear functions, Φ is a vector containing the nodal values of the steady potential Φ, and $\mathbf{X}$ is a vector containing the x and y coordinates of each node of the grid.

Since, the unsteady rotational velocity $\mathbf{v}^R$ is fundamentally dependent on the drift and stream functions, it is convenient to perform our numerical calculations on a streamline computational grid. However, one cannot know the position of streamlines *a priori*. Therefore, we must generate the computational grid as part of the steady solution procedure. We use a modified elliptic grid generation technique originally proposed by Thompson *et al.* (1977), but modified to ensure that the resulting streamwise grid lines are true streamlines. When discretized, the grid equations are of the form

$$\mathbf{M}(\Phi, \mathbf{X}) = 0 \qquad (42)$$

where $\mathbf{M}$ is a vector of nonlinear grid generation equations, two for each node of the grid.

Equations (41) and (42) are solved simultaneously using Newton iteration to determine the steady velocity potential Φ and the grid geometry $\mathbf{X}$. Typically, about four Newton iterations are required to obtained a converged steady solution. A trivial computation is then required to compute the stream function Ψ and drift function Δ at each node of the grid. For typical problems using a 129×33 computational grid, the steady solution procedure requires on the order of 25 minutes of computer time per blade row using a Silicon Graphics Indigo (R4400) workstation.

2.2.3. Numerical Solution of the Unsteady Flow Field. Next, the small disturbance unsteady flow equations are discretized. First, for vortical gust problems, the rotational velocity $\mathbf{v}^R$ is computed analytically at the nodes of the computational grid using Eq. (40). Then, Eq. (39) is discretized using a variational finite element technique developed by Hall (1993). The finite element code has a number of important features. For instance, complex periodicity, Eq. (5), is imposed, allowing the computational domain to be reduced to a single blade passage, thereby reducing the computational effort required to compute flows with nonzero interblade phase angles. Also, to prevent spurious reflections of acoustic and vortical waves, numerically exact nonreflecting boundary conditions are applied at the far-field boundaries of the computational domain. Finally, for aerodynamic damping calculations, a deforming computational grid which conforms to the motion of the airfoil is used to improve the accuracy of the scheme.

When assembled, the discretized equations governing the unsteady small disturbance flow have the form

$$[\mathbf{A}]\{\phi\} = \{\mathbf{b}\} \qquad (43)$$

where $\mathbf{A}$ is a sparse complex matrix which is a function of the frequency ω and interblade phase angle σ. The vector $\mathbf{b}$ arises from the imposition of an external disturbance, e.g. an incident acoustic wave or a prescribed blade motion. Note that the number of unknowns in Eq. (43) is about one-third that in Eqs. (41) and (42) since no grid generation equations must be solved for the unsteady flow problem. The matrix $\mathbf{A}$ is factored into a product of upper and lower triangular matrices (LU factorization). In this way, the unsteady solution for several different external disturbances at the same interblade phase angle and frequency (different $\mathbf{b}$'s) can be computed very efficiently, each requiring just one forward and one backward matrix substitution. Typically, the reflection/transmission coefficients for a single scatter group can be computed in less than one minute.

The above description of the numerical model used to compute the steady and unsteady aerodynamic characteristics of the individual blade rows is, because of space limitations, quite terse. The interested reader is referred to Hall (1993), Lorence & Hall (1996), and Silkowski (1996) for additional details on the method, and also numerical examples used to validate the method.

3. RESULTS

In this section, we consider the unsteady aerodynamic response of a compressor cascade which is part of a multistage compressor. In particular, we consider two geometries. The first, Configuration C, is a one and one-half stage compressor whose airfoils are flat plates which do no steady turning. The second, Configuration D, is a two and one-half stage section of a two-dimensional

Table 1: Cascade parameters for Configuration C, a one and one-half stage compressor composed of flat-plate airfoils.

Station or Row	0	1	2	3
Type of Blade Row	—	Stator	Rotor	Stator
Number of Blades, B	—	3	4	5
Chord	—	1.261	1.0	0.820
Circumferential Gap, G	—	1.067	0.8	0.64
Stagger Angle, Θ (deg)	—	37.5	-60.0	37.5
Axial Gap, Δx	—	0.125	0.125	—
V_{rel}	1.000	1.000	1.000	1.000
V_{abs}	0.630	0.630	0.630	0.630
M	0.0	0.0	0.0	0.0
Flow Angle, α_{rel} (deg)	-60.0	-60.0	-60.0	-60.0
Flow Angle, α_{abs} (deg)	37.5	37.5	37.5	37.5
Static Density, $\overline{\rho}$	1.000	1.000	1.000	1.000

compressor with 'real' blades, i.e. the blades have thickness and camber and do steady turning.

3.1. Multistage Configuration C

To validate the coupled mode analysis, we first consider a one and one-half stage compressor composed of flat plate airfoils which do no steady turning. The geometry for this multistage machine is given in Table 1. In particular, the ratio of blades in the three blade rows is 3:4:5, and the axial gap between blade rows is quite small, approximately 20% of the blade chord. Note that lengths have been nondimensionalized by the aerodynamic chord c of the rotor blades of the middle blade row, velocities by the relative inflow velocity to the rotor, and pressures by the quantity $\overline{\rho}V_{\text{rel}}^2$.

The airfoils of the rotor (the middle blade row) are prescribed to vibrate in plunge with a reduced frequency ω_0 of 0.5 and an interblade phase angle σ_0 of 90°. The unsteady aerodynamic response was then computed in two ways. First, we applied the present coupled mode analysis described in this paper, but with Whitehead's (1987) LINSUB code used to compute the reflection/transmission coefficients of the individual blade rows. LINSUB was used here because it is essentially exact. Thus, any errors will be due to the coupled mode analysis itself, and not truncation error of the aerodynamic code. To couple the blade rows, we used one, 11, and 27 spinning modes. The mode order indices associated with these spinning modes are shown in Table 2. For the 11-mode case, for example, we used the first 11 modes in the table. The selection of spinning modes used is somewhat of an art. Generally, spinning modes are selected which have a relatively small number of nodal diameters, since these low-order modes tend to be cut-on or are weakly cut-off. Also used are some spinning modes which may have a larger number of nodal diameters, but are members of the fundamental mode's scatter group, and also provide a kinematic connection between the fundamental and low-order spinning modes.

We also used an incompressible time-marching vortex-lattice

Table 2: Indices of spinning modes used for coupled mode analysis of multistage compressors. $N = n_1B_1 + n_2B_2 + n_3B_3$.

Mode	(n_1, n_2, n_3)	Mode	(n_1, n_2, n_3)
1	(0, 0, 0)	14	(-1,-2,+1)
2	(0,-1, 0)	15	(+1,-2, 0)
3	(-1, 0, 0)	16	(-1,+1,-1)
4	(0,+1,-1)	17	(0,+2, 0)
5	(+1,-1, 0)	18	(0,-2,+1)
6	(0, 0,-1)	19	(+1, 0,-1)
7	(-1,+1, 0)	20	(-1,+2,-1)
8	(0,-1,+1)	21	(+1,-2,+1)
9	(+1, 0, 0)	22	(-1, 0,+1)
10	(0,+1, 0)	23	(0,+2,-1)
11	(0, 0,+1)	24	(+1,-1,+1)
12	(-1, 0,-1)	25	(-1,+2, 0)
13	(0,-2, 0)	26	(+1,+2,-1)
		27	(+1, 0,+1)

code developed by Silkowski (1996) to compute the unsteady lift acting on the compressor blades. Using this approach, the blades and wakes of the cascades are modelled by vortex elements. At the quarter-chord of each element is placed a discrete vortex. At the three-quarter-chord of each element on the airfoils is a collocation point. To start the calculation, the strengths of all the vortex elements are set to zero. Then, at each time step, the strengths of the vortex elements on the airfoils are selected so that the no-through-flow condition is satisfied. The strength of the first vortex element in the wake of each airfoil is chosen so as to satisfy Kelvin's theorem, i.e. the circulation about a fixed set of fluid particles is constant. The vorticity in the remainder of the wake is simply convected with the mean flow velocity. After each time step, the position of the rotor is incremented, and the entire process is repeated. For this example, we divided each airfoil of the three blade rows into 80, 40, and 52 vortex elements, respectively. At this resolution, the resulting unsteady lift computation was found to be element converged, that is, the unsteady lift is nearly identical to that predicted using half as many elements per airfoil.

Shown in Fig. 3 is the computed unsteady lift acting on the three blade rows as a function of time. These results were computed using the coupled mode analysis with one, 11, and 27 spinning modes. (The 27-mode solution is nearly identical to the 11-mode solution, and is omitted from the figure for clarity.) Also shown is the unsteady lift calculated using the vortex-lattice time-domain simulation. Here the lift is nondimensionalized by $\overline{\rho}V_{\text{rel}}\dot{h}_0 c$, where $\overline{\rho}$ is the mean static density, V_{rel} is the mean flow velocity as viewed in the blade row's frame of reference, c is the chord of the airfoils in the specified row, and $\dot{h}_0$ is the amplitude of plunging of the rotor blades.

After the initial transients associated with the start-up of the vortex-lattice simulation have subsided, the agreement between the vortex-lattice simulation and the coupled mode analysis is quite

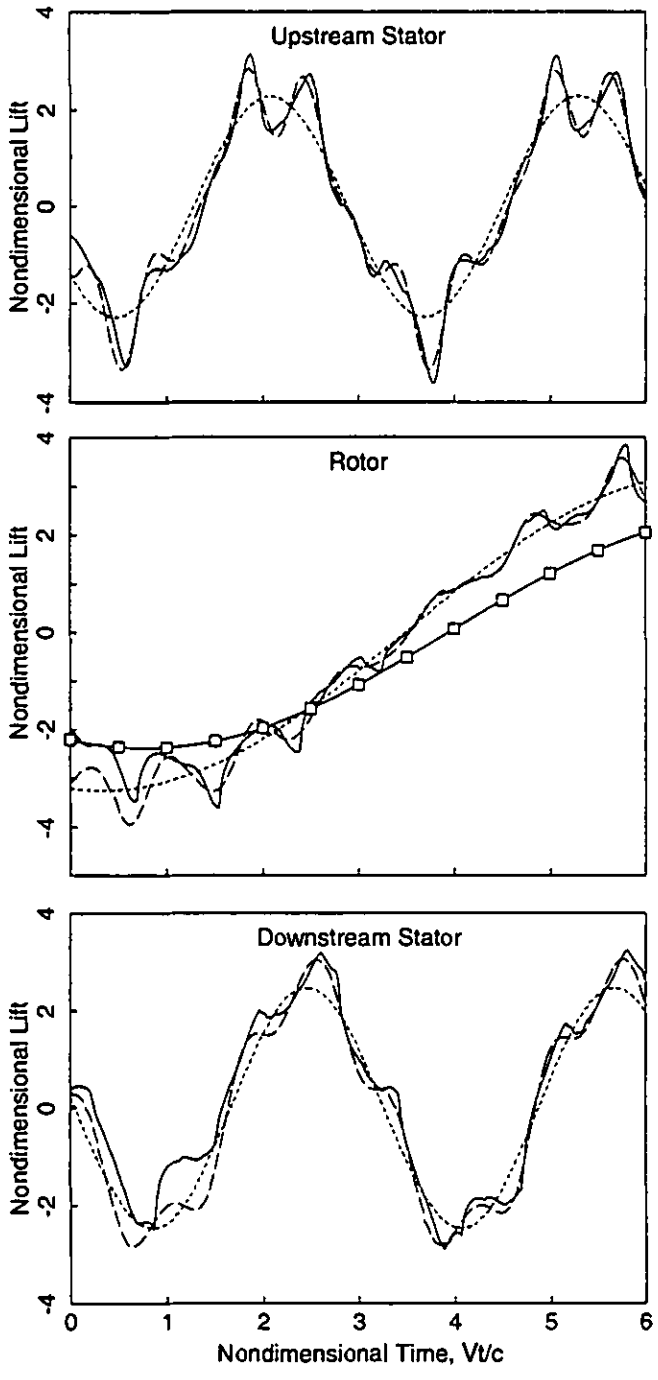

Figure 3: Unsteady lift histories on the reference airfoils of Configuration C (stator/rotor/stator). Rotor blades vibrate in plunge with σ_0 = 90°, ω_0 = 0.5. ——□——, uncoupled; - - - - -, one mode; — — —, 11 modes; ———, vortex-lattice code.

good, especially for the 11-mode case. The minor discrepancies are seen to have a high frequency content. The agreement is not exact because only a finite number of the infinite number of spinning modes which participate in the solution have been included in the coupled mode model. Nevertheless, even the one-mode case

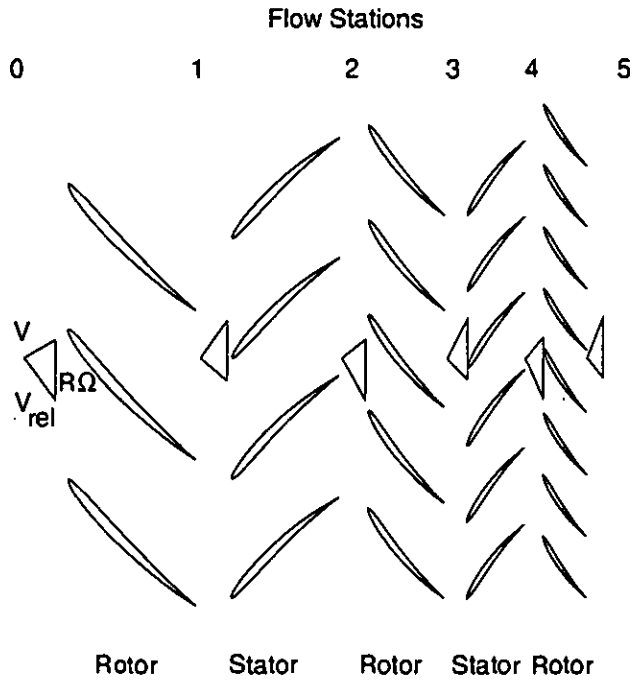

Figure 4: Configuration D, a two-dimensional, two and one-half stage compressor with rows of NACA four digit series airfoils.

shows the correct low-frequency behavior (this frequency corresponds to the original blade vibration frequency). These results demonstrate several important points. First, a small number of the infinite set of possible spinning modes provide most of the coupling between the blade rows. Second, the coupled mode analysis exhibits mode convergence. As more spinning modes are included in the model, the solution converges to the exact solution. Third, if one is interested in the response at the original excitation frequency, e.g. for aerodynamic damping calculations, then engineering accuracy results may be obtained with as few as one spinning mode. Fourth, and finally, the unsteady aerodynamic response of the rotor to blade vibration is significantly altered by the presence of neighboring blade rows.

3.2. Multistage Configuration D

Having validated the coupled mode analysis for incompressible flows, we next consider compressible flows in the two and one-half stage compressor section shown in Fig. 4, denoted here as Configuration D. The airfoils of each blade row of the compressor are NACA four digit series airfoils. In most instances, we will calculate the unsteady flow through the middle three blade rows of this configuration (one and one-half stages). Later, the first and last blade rows will be included to create a full two and one-half stage machine. As shown in Fig. 4, the blade rows are closely spaced, as is typical in modern compressors. The specific geometry for the compressor is given in Table 3. As before, lengths have been nondimensionalized by the aerodynamic chord c of the rotor blades of the middle rotor, velocities by the relative inflow velocity V_{rel} at Station 2, and pressures by the quantity $\bar{\rho}V_{rel}^2$ at Station 2.

Shown in Fig. 5 is the computed steady pressure distribution on

Table 3: Cascade parameters for Configuration D, a two and one-half stage compressor composed of NACA four digit series airfoils.

Station or Row	0	1	2	3	4	5
Type of Blade Row	—	Rotor	Stator	Rotor	Stator	Rotor
Number of Blades, B	—	26	32	40	50	62
NACA 4-Digit Airfoil	—	(3.5)506	(4.5)506	(4.5)506	(4.5)506	(4.5)506
Chord	—	1.539	1.25	1.0	0.8	0.645
Circumferential Gap, G	—	1.231	1.0	0.8	0.64	0.516
Axial Gap, Δx	—	0.31	0.25	0.20	0.16	—
V_{rel}	1.112	0.744	1.000	0.609	0.919	0.531
V_{abs}	0.780	0.959	0.630	0.926	0.562	0.906
M_{rel}	0.829	0.535	0.700	0.414	0.609	0.344
M_{abs}	0.581	0.689	0.441	0.629	0.373	0.586
Flow Angle, α_{rel} (deg)	–52.0	–40.0	–60.0	–45.0	–65.5	–50.5
Flow Angle, α_{abs} (deg)	28.6	53.5	37.5	62.3	47.3	68.1
Stagger Angle, Θ (deg)	—	–44	43	–49.5	52	–55
Static Pressure, P	0.939	1.213	1.458	1.797	2.131	2.524
Total Pressure, $P_{T,rel}$	1.473	1.473	2.022	2.022	2.739	2.739
Total Pressure, $P_{T,abs}$	1.180	1.666	1.666	2.346	2.346	3.185

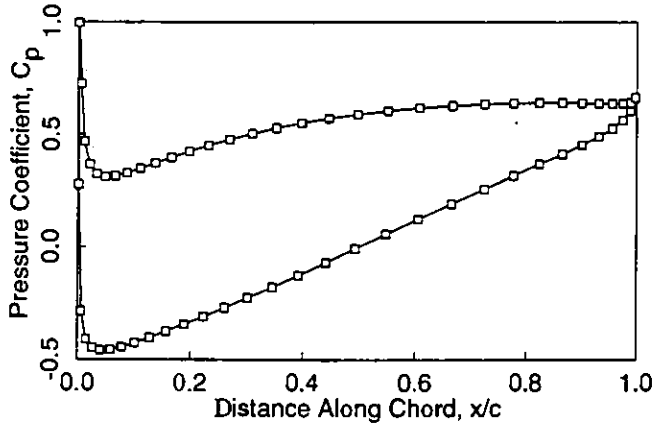

Figure 5: Steady pressure distribution on surface of airfoils of middle rotor of Configuration D compressor at design conditions.

the surface of the blades of the middle blade row. The grid used for this calculation was an H-grid with 129×33 grid points (129 nodes in the streamwise direction, and 33 nodes in the normal direction). This same grid resolution was used to compute the steady and unsteady flow solutions in all the blade rows. For the cases considered in this paper, the flow throughout the multistage compressor is entirely subsonic.

The first unsteady example considered for Configuration D is an aerodynamic damping calculation where the middle three blade rows (one and one-half stages) are retained in the model. The blades of the middle rotor are prescribed to vibrate in plunge normal to the blade chord with a reduced frequency ω_0 of 0.5 for a range of interblade phase angles σ_0. The unsteady aerodynamic response was computed using the coupled mode analysis with zero, one, 11, and 27 spinning modes (see Table 2). The zero mode case corresponds to an isolated blade row (no inter-row coupling).

Figure 6 shows the computed unsteady pressure on the surface of the reference blade of the rotor for the case where a single mode is used to couple the three blade rows. Also shown is the pressure distribution for the uncoupled case. Here, the pressure is nondimensionalized by $\bar{p}V\dot{h}_0$, where $\bar{p}$ and V are the mean static density and flow velocity as viewed in the rotor's frame of reference, and $\dot{h}_0$ is the amplitude of the plunging velocity of the reference blade of the rotor. Using this nondimensionalization, it is the real part of the unsteady pressure that contributes to aerodynamic damping. Note that the coupled and uncoupled pressure distributions differ substantially. In this case, the damping of the rotor in the presence of the neighboring stators is much larger than the damping of the same rotor isolated in an infinitely long duct.

One can integrate the unsteady pressure distribution on the surface of the airfoil to obtain the unsteady lift. Figure 7 shows the real and imaginary part of the computed unsteady lift. In general, the unsteady lift will contain many frequencies due to the scattering of modes and subsequent shifting of frequencies. However, we have plotted only the component of the lift which has the same frequency and interblade phase angle as the blade motion since this is the only part which does modal work on the vibrating airfoils, and hence is the only part which contributes to aerodynamic damping. The unsteady lift is nondimensionalized by $\bar{p}V_{rel}\dot{h}_0 c$ where the steady flow quantities are taken to be those at Station 2, c is the chord of the middle rotor, and $\dot{h}_0$ is the amplitude of the plunging velocity of the reference rotor blade. Using this nondimensionalization, the aerodynamic damping is negative whenever the real part of the lift is greater than zero.

For small interblade phase angles, the presence of the stators

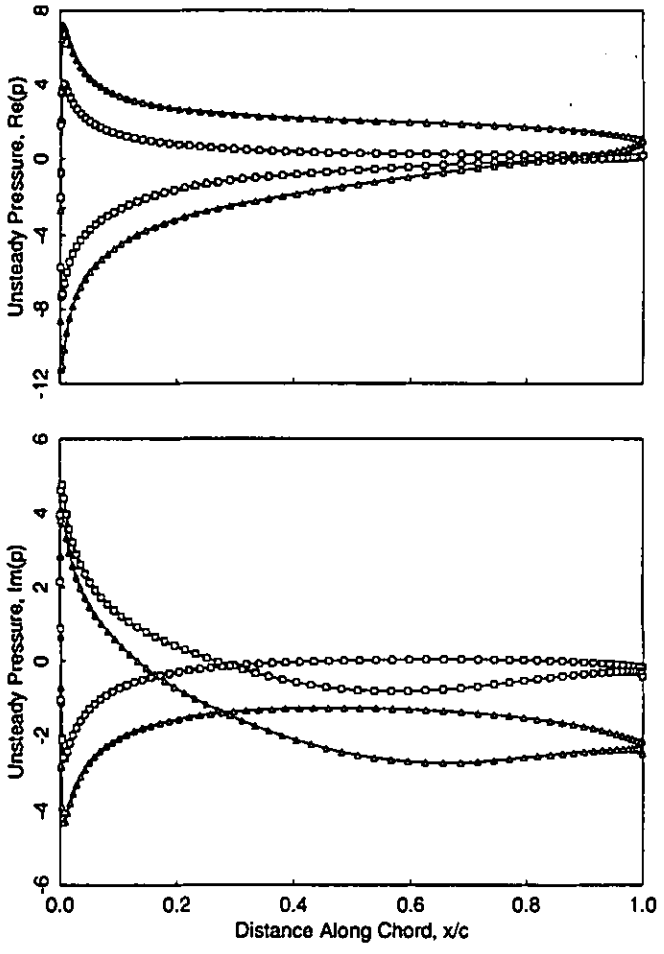

Figure 6: Fundamental harmonic of unsteady surface pressure on reference airfoil of middle rotor of Configuration D. Three blade row case, plunging excitation with (σ_0,ω_0) = (60°,0.5). —□—, uncoupled; —△—, one mode coupling.

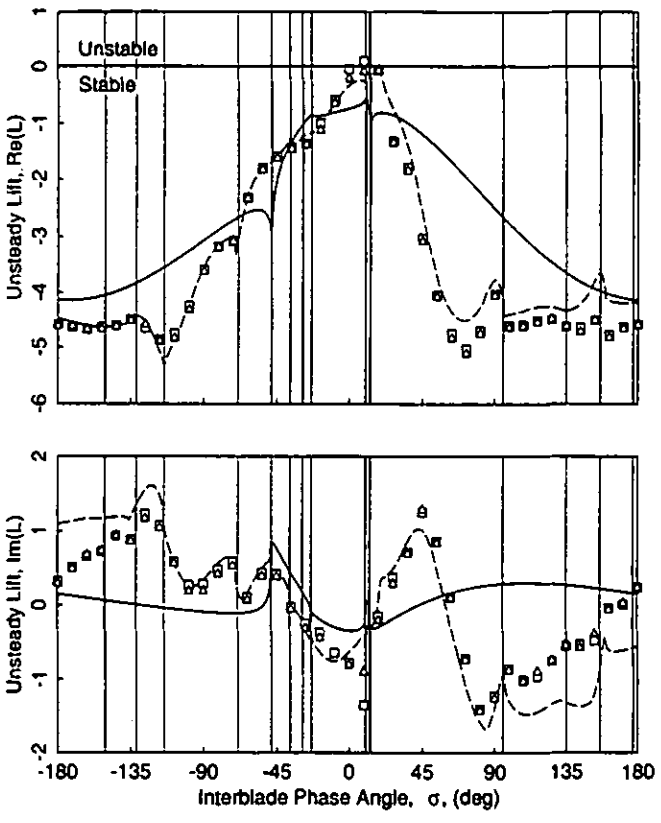

Figure 7: Fundamental harmonic of unsteady lift acting on reference airfoil of middle rotor of Configuration D. Three blade row case, plunging excitation with ω_0 = 0.5. ———, uncoupled; — — —, one mode; □, 11 modes; △, 27 modes.

has had an aeroelastically destabilizing effect on the rotor. In other regions, for example near an interblade phase angle σ_0 of 60°, the isolated blade row calculation seriously under predicts the aerodynamic damping. This is an important result. *The aerodynamic damping of a blade row which is part of a multistage machine can be significantly different than that predicted using an isolated blade row model.*

The results shown in Fig. 7 demonstrate that the Coupled Mode Method displays mode convergence, i.e. as the number of spinning modes in the model is increased, the computed unsteady lift converges to a fixed value. Furthermore, only a relatively small number of spinning modes need to be retained to obtain good estimates of the aerodynamic damping. In fact, for this example, engineering accuracy is achieved with just one mode.

Another interesting feature of Fig. 7 is that the coupled unsteady aerodynamic damping curves have numerous slope discontinuities, whereas the uncoupled aerodynamic damping curve has just four. For the uncoupled (isolated blade row) case, these discontinuities correspond to the four interblade phase angles at which duct modes are cut on (acoustic resonances) upstream and downstream of the blade row for the prescribed blade vibration frequency. For the coupled case, many more acoustic resonance points appear. These new resonance points appear for at least three reasons. First, there are now multiple frequencies present in the response due to frequency shifting. There will thus be new sets of acoustic resonances for each discrete frequency in the response. Second, because of mode scattering, waves of multiple wavelengths are set up in the duct. Whenever one of these scattered waves passes through a resonance, the transmission/reflection coefficients of the blade rows adjacent to that section of the duct will abruptly change. Third, each blade row does mean turning of the flow causing each of the inter-row flow regions to have different properties, including acoustic resonance points. The acoustic resonance points of the one and one-half stage compressor are identified with vertical lines in Fig. 7. Overall, the agreement between the predicted and computed resonance points is quite good. The lack of agreement at some of the higher interblade phase angles may be due to a lack of grid resolution required to analyze spinning modes with high frequencies and short wavelengths. This problem is not a deficiency of the coupled mode analysis, but rather truncation error associated the individual blade row flow solver (this problem also occurs with time-marching codes).

Next, to determine the relative importance of multistage effects compared to real blade effects (camber, thickness, etc.), we defined

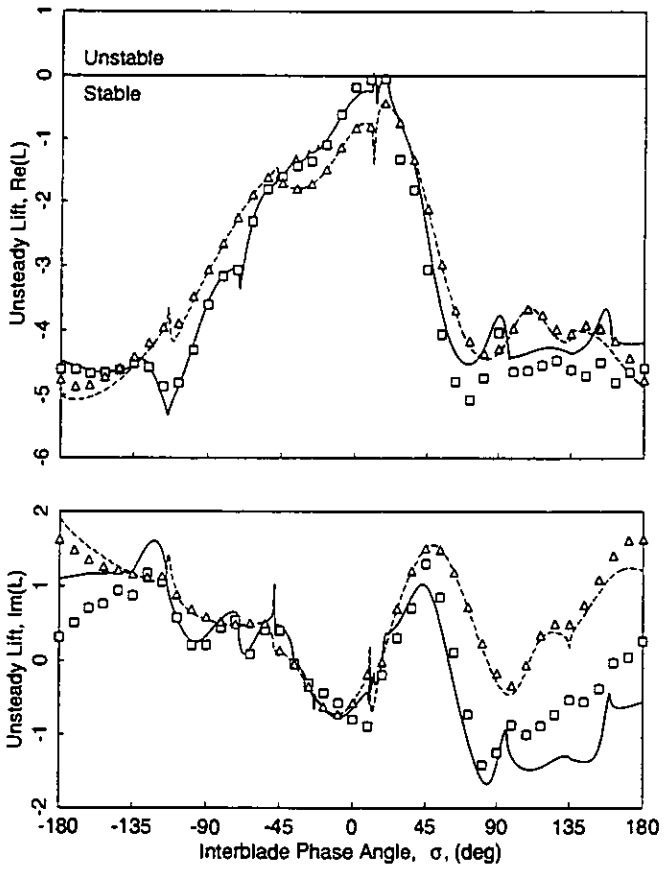

Figure 8: Fundamental harmonic of unsteady lift acting on reference airfoil of middle rotor of one and one-half stage compressor. Three blade row case, plunging excitation with ω_0 = 0.5. Configuration D: ————, one mode; □, 27 modes. equivalent flat-plate compressor: — — —, one mode; △, 27 modes.

an 'equivalent flat-plate compressor.' This compressor is similar to Configuration D, except that the airfoils in each row have been replaced with flat plates with the same aerodynamic chord. The equivalent flat-plate compressor does no work on the fluid. Thus, the mean flow is uniform with flow properties equal to those at Station 2 (the inlet conditions to the reference rotor) of Configuration D. Finally, the stagger angles of the blades are adjusted to be aligned with the relative mean flow in each blade row. Shown in Fig. 8 is the computed unsteady lift for Configuration D and the Equivalent Flat-Plate Compressor for plunging motion of the middle rotor blade with a reduced frequency ω_0 of 0.5. As expected, the unsteady lifts for these two configurations differ somewhat. However, the differences are smaller than the differences between the coupled and uncoupled solutions of Configuration D (see Fig. 7). In other words, *multistage effects can have a larger impact on aerodynamic damping than real blade effects.*

If multistage effects can indeed influence the aerodynamic damping of a rotor, as suggested by the previous results, then it may be possible to use the axial spacing between blade rows as a passive means for improving the aeroelastic performance of a rotor. Figure 9 shows the real part of the unsteady lift for Configuration D

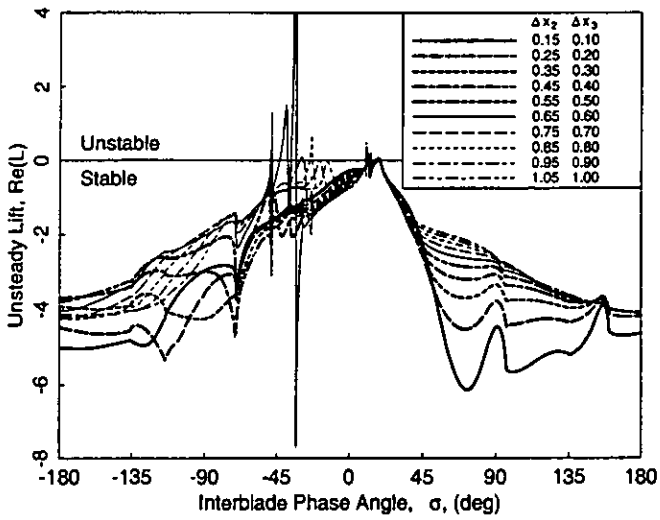

Figure 9: Fundamental harmonic of unsteady lift acting on reference airfoil of middle rotor of Configuration D for various axial spacings between blade rows. Three blade row case, plunging excitation with ω_0 = 0.5.

due to plunging motion of the middle rotor as before, but for several values of axial spacing between the rotor and the neighboring stators (these results were computed using one mode coupling). As the axial gaps are varied, the unsteady lift (aerodynamic damping) takes on a wide range of values.

Finally, we consider the influence of blade rows beyond the two neighboring stators. For this final example, we include the upstream and downstream rotors of Configuration D. Figure 10 shows the computed unsteady lift where all five blade rows have been modelled (we also show the isolated blade row model and the previous three blade row model for comparison). Eleven spinning modes were used to couple the blade rows. Over most of the interblade phase angle range, the three and five blade row solutions are nearly the same. For interblade phase angles between about 20° and 100°, however, the addition of the outer two rotors has a modest influence on the aerodynamic damping of the middle rotor. Nevertheless, the nearest two stators clearly have the strongest influence on the unsteady aerodynamic behavior of the rotor. Hall and Silkowski (1995) have shown that additional blade rows (beyond five) have very little influence on the unsteady lift on the middle rotor. The physical explanation for this is that vortical and acoustic waves tend to be diminished as they travel from one blade row to the next. This is because transmission and reflection coefficients are usually less than unity. Furthermore, many of the acoustic waves are cut-off.

3.3. Computational Requirements

The computational time t_{cpu} required to solve a series of unsteady multistage problems can be approximated by

$$t_{\text{cpu}} \approx M \cdot (t_s + M_p M_m t_u) \tag{44}$$

where M is the number of blade rows, M_m is the number of spinning modes used in the multistage calculations, M_p is the number

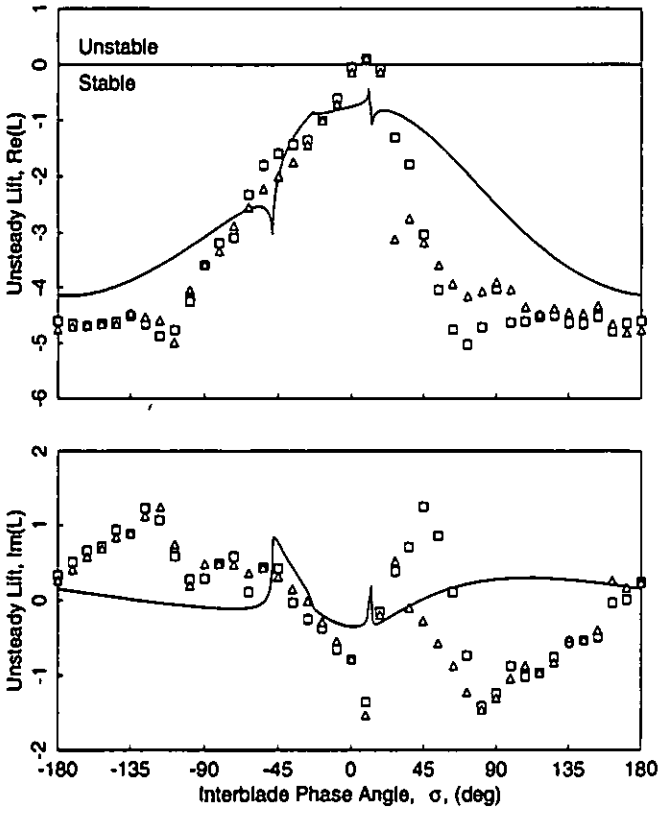

Figure 10: Fundamental harmonic of unsteady lift acting on reference airfoil of middle rotor of Configuration D for plunging excitation with ω_0 = 0.5. ———, uncoupled; △, three blade rows; □, five blade rows.

of original interblade phase angles σ_0 and/or frequencies ω_0 considered, t_s is the computational time required to compute the steady flow in a single blade row, and t_u is the computational time required to compute the unsteady response of a single blade row to unsteady excitations of a single spinning mode. As an example, consider the results shown in Fig. 7 computed using 11 spinning modes (M_m = 11). For this example M = 3 and M_p = 41. Using a Silicon Graphics Indigo (R4400) workstation, we found that t_s = 1475 sec and t_u = 51 sec. Thus, to generate all of the 11 spinning mode results shown in Fig. 7 required approximately 20.4 hr of CPU time.

4. SUMMARY AND CONCLUSIONS

In this paper, we have presented a coupled mode analysis – a technique for calculating the unsteady aerodynamic response of a blade row which is embedded in a multistage machine. Using this approach, the problem is first subdivided into a number of simpler problems, that is, finding the response of the individual blade rows in isolation at a number of frequencies and interblade phase angles. These individual solutions are then used to form a fairly small sparse matrix equation which describes the unsteady aerodynamic response of the multistage machine.

Based on the numerical results computed to date, we can make the following conclusions and observations.

1) The aerodynamic damping of a blade row which is part of a multistage machine can be significantly different than that predicted using an isolated blade row model. This is an important result since virtually all unsteady aerodynamic theories currently used in industry assume that the blade row can be modelled as isolated in an infinitely long duct.

2) A good estimate of the aerodynamic damping can be obtained using just a few spinning modes in the model. In fact, most of the unsteady aerodynamic coupling between blade rows occurs in the fundamental spinning mode, that is, the spinning mode associated with the original disturbance. Scattered modes are relatively less important.

3) For a typical compressor geometry, multistage effects can have a larger impact on aerodynamic damping than real blade effects. (This may not be true in the case of turbine blades, where the turning is much larger.) Given the state of the art in unsteady aerodynamic theories, this suggests that more effort should be devoted to understanding multistage physics.

4) The two neighboring stator blade rows adjacent to a rotor have the strongest influence on the unsteady aerodynamic response of the rotor. The next nearest blade rows are less important, but can still have a modest influence.

5) The coupled mode analysis is computationally very efficient. For example, to compute the aerodynamic damping of a rotor embedded in a one and one-half stage compressor section (Configuration D) at a single reduced frequency and interblade phase angle using a single spinning mode required just 153 sec of CPU time on a Silicon Graphics Indigo (R4400) workstation.

6) The coupled mode analysis is flexible and well-suited for certain parametric design studies. For example, once the reflection/transmission coefficients have been calculated for each of the blade rows of a given multistage machine, it is very inexpensive to recompute the aerodynamic damping for a range of axial or circumferential spacings between blade rows, or to compute the response to an incident wake instead of a prescribed blade vibration. Furthermore, because of the modular nature of the method, if a single blade row of a multistage machine is redesigned, one need only recompute the reflection/transmission coefficients for the redesigned blade row, and then solve the small global matrix equation. Conventional time-marching simulations, on the other hand, would require a completely new computation of the entire multistage machine for any variation in geometry or excitation.

7) It may be possible to use the multistage influence on aerodynamic damping to good effect. For instance, it may be possible in some cases to increase the aerodynamic damping of a rotor by altering the axial spacing between adjacent blade rows.

Finally, we would comment that while the analysis presented in this paper has been entirely two-dimensional, we expect that multistage effects will strongly influence unsteady flows in real turbomachines, which are fundamentally three-dimensional. Indeed, unlike steady flows, which can to a good approximation be computed using two-dimensional isolated blade row techniques, accurate predictions of unsteady flows will likely require a three-dimensional multistage analysis. The authors are currently extending the present coupled mode analysis to three-dimensional flows.

ACKNOWLEDGMENTS

This material is based upon work supported by the National Science Foundation under Grant No. CTS-9157908. The government has certain rights in this material. The authors would like to thank Dr. Christopher B. Lorence for his help in developing the linearized potential/rapid distortion theory model used in this study, and Dr. Donald B. Hanson for many helpful discussions on mode coupling.

REFERENCES

Adamczyk, J. J., & Goldstein, M. E., 1978, "Unsteady Flow in a Supersonic Cascade With Subsonic Leading Edge Locus," AIAA Journal, Vol. 16, No. 12, pp. 1248–1254.

Atassi, H. M., & Grzedzinski, J., 1989, "Unsteady Disturbances of Streaming Motions Around Bodies," Journal of Fluid Mechanics, Vol. 209, December, pp. 385–403.

Bateman, H., 1930, "Irrotational Motion of a Compressible Fluid," Proceedings of the National Academy of Sciences, Vol. 16, pp. 816–825

Bölcs, A., & Fransson, T. H., 1986, "Aeroelasticity in Turbomachines. Comparison of Theoretical and Experimental Cascade Results," AFOSR–TR–0605, Air Force Office of Scientific Research, Washington, DC.

Buffum, D. H., 1993, "Blade Row Interaction Effects on Flutter and Forced Response," AIAA Paper No. 93-2084.

Clark, W. S., & Hall, K. C., 1995, "A Numerical Model of the Onset Stall Flutter in Cascades," ASME Paper No. 95-GT-377.

Gerolymos, G. A., 1993, "Advances in the Numerical Integration of the Three-Dimensional Euler Equations in Vibrating Cascades," ASME Journal of Turbomachinery, Vol. 115, No. 4, pp. 781–790.

Giles, M. B., 1988a, "Calculation of Unsteady Wake/Rotor Interaction," AIAA Journal of Propulsion, Vol. 4, No. 4, pp. 356–362.

Giles, M. B., 1988b, "Stator/Rotor Interaction in a Transonic Turbine," AIAA Paper No. 88–3093.

Goldstein, M. E., 1978, "Unsteady Vortical and Entropic Distortions of Potential Flows Round Arbitrary Obstacles," Journal of Fluid Mechanics, Vol. 93, Part 3, pp. 433–468.

Hall, K. C., 1993, "Deforming Grid Variational Principle for Unsteady Small Disturbance Flows in Cascades," AIAA Journal, Vol. 31, No. 5, pp. 891–900.

Hall, K. C., & Clark, W. S., 1993, "Linearized Euler Prediction of Unsteady Aerodynamic Loads in Cascades," AIAA Journal, Vol. 31, No. 3, pp. 540–550.

Hall, K. C., & Crawley, E. F., 1989, "Calculation of Unsteady Flows in Turbomachinery Using the Linearized Euler Equations," AIAA Journal, Vol. 27, No. 6, pp. 777-787.

Hall, K. C., & Lorence, C. B., 1993, "Calculation of Three-Dimensional Unsteady Flows in Turbomachinery Using the Linearized Harmonic Euler Equations," ASME Journal of Turbomachinery, Vol. 115, No. 4, pp. 800-809.

Hall, K. C., & Silkowski, P. D., 1995, "The Influence of Neighboring Blade Rows on the Unsteady Aerodynamic Response of Cascades," ASME Paper No. 95–GT–35.

Hall, K. C., & Verdon, J. M., 1991, "Gust Response Analysis for Cascades Operating in Nonuniform Mean Flows," AIAA Journal, Vol. 29, No. 9, pp. 1463–1471.

Hanson, D. B., 1992, "Unsteady Coupled Cascade Theory Applied to the Rotor/Stator Interaction Noise Problem," DGLR/AIAA Paper No. 92–02–084.

Hanson, D. B., 1993, "Mode Trapping in Coupled 2D Cascades – Acoustic and Aerodynamic Results," AIAA Paper No. 93–4417.

He, L., 1990, "An Euler Solution for Unsteady Flows Around Oscillating Blades," ASME Journal of Turbomachinery, Vol. 112, No. 4, pp. 714–722

Holmes, D. G., & Chuang, H. A., 1993, "2D Linearized Harmonic Euler Flow Analysis for Flutter and Forced Response," Unsteady Aerodynamics, Aeroacoustics, and Aeroelasticity of Turbomachines and Propellers, H. M. Atassi (ed.), Springer-Verlag, New York. (Originally presented 1991.)

Huff, D. L., Swafford, T. W., & Reddy, T. S. R., 1991, "Euler Flow Predictions for an Oscillating Cascade Using a High Resolution Wave–Split Scheme," ASME Paper No. 91–GT-198.

Kaji, S., and Okazaki, T., 1970, "Generation of Sound by Rotor-Stator Interaction," Journal of Sound and Vibration, Vol. 13, No. 3, pp. 281–307.

Lighthill, M. J., 1956, "Drift," Journal of Fluid Mechanics, Vol. 1, May, pp. 31–53.

Lorence, C. B., & Hall, K. C., 1996, "Sensitivity Analysis of the Aeroacoustic Response of Turbomachinery Blade Rows," AIAA Journal, Vol. 34, No. 8, pp. 1545–1554.

Marshall, J. G., & Imregun, M., 1996, "A Review of Aeroelasticity Methods with Emphasis on Turbomachinery Applications," Journal Fluids and Structures, Vol. 10, No. 3, pp. 237–267.

Nagashima, T. & Whitehead, D. S., 1977 "Linearized Supersonic Unsteady FLow in Cascades," Reports and Memoranda No. 3711, Aeronautical Research Council, London.

Rai, M. M.,1989a, "Three-Dimensional Navier-Stokes Simulations of Turbine Rotor-Stator Interaction, Part I – Methodology," Journal of Propulsion and Power, Vol. 5, No. 3, pp. 305–311.

Rai, M. M., 1989b, "Three-Dimensional Navier-Stokes Simulations of Turbine Rotor-Stator Interaction, Part II – Results," Journal of Propulsion and Power, Vol. 5, No. 3, pp. 312–319.

Silkowski, P. D., 1996, "A Coupled Mode Method for Multistage Aeroelastic and Aeroacoustic Analysis of Turbomachinery," Ph.D. Thesis, Duke University, Durham, NC.

Smith, S. N., 1972, "Discrete Frequency Sound Generation in Axial Flow Turbomachines," Reports and Memoranda No. 3709, Aeronautical Research Council, London.

Thompson, J. F., Thames, F. C., & Mastin, C. W., 1977, 'A Code for Numerical Generation of Boundary-Fitted Curvilinear Coordinate Systems on Fields Containing any Number of Arbitrary Two-Dimensional Bodies," Journal of Computational Physics, Vol. 24, No. 3, pp. 274–302.

Verdon, J. M., 1987, "Linearized Unsteady Aerodynamic Theory," in: AGARD Manual on Aeroelasticity in Axial Flow Turbomachines, Volume 1, Unsteady Turbomachinery Aerodynamics (AGARD-AG-298), M. F. Platzer and F. O. Carta, ed., Neuilly sur Seine, France, ch. 2.

Verdon, J. M., 1993, "Review of Unsteady Aerodynamic Methods for Turbomachinery Aeroelastic and Aeroacoustic Applications," AIAA Journal, Vol. 31, No. 2, pp. 235–250.

Verdon, J. M., & Caspar, J. R., 1982, "Development of a Linear Unsteady Aerodynamic Analysis for Finite-deflection Subsonic

Cascades," AIAA Journal, Vol. 20, No. 9, pp. 1259-1267.

Verdon, J. M., & McCune, J. E., 1975, "Unsteady Supersonic Cascade in Subsonic Axial Flow," AIAA Journal, Vol. 13, No. 2, pp. 193–201.

Whitehead, D. S., 1960, "Force and Moment Coefficients for Vibrating Aerofoils in Cascade," Reports and Memoranda No. 3254, Aeronautical Research Council, London.

Whitehead, D. S., 1970, "Vibration and Sound Generation in a Cascade of Flat Plates in Subsonic Flow," Reports and Memoranda No. 3685, Aeronautical Research Council, London.

Whitehead, D. S., 1987, "Classical Two-Dimensional Methods," in: AGARD Manual on Aeroelasticity in Axial Flow Turbomachines, Volume 1, Unsteady Turbomachinery Aerodynamics (AGARD-AG-298), M. F. Platzer and F. O. Carta, ed., Neuilly sur Seine, France, ch. 3.

Whitehead, D. S., 1990, "A Finite Element Solution of Unsteady Two-Dimensional Flow in Cascades," International Journal for Numerical Methods in Fluids, Vol. 10, No. 1, pp. 13-34.